Energy Conversion and Management 356 (2026) 121350

Contents lists available at ScienceDirect

Energy Conversion and Management

journal homepage: www.elsevier.com/locate/enconman

Experimental study on the combustion of methane-hydrogen mixtures in a pilot-scale furnace☆

Jorge Arroyo [a,*], Fabiola Tovar-Lasheras [a], Antonia Gil [b]

[a] CIRCE Technology Center, Parque Empresarial Dinamiza Avenida Ranillas, 3D 1ª Planta, 50018 Zaragoza, Spain
[b] Universidad de Zaragoza, IUI mixto ENERGAIA, Campus Río Ebro, Mariano Esquillor Gómez, 15, 50018 Zaragoza, Spain

ARTICLE INFO

Keywords:
Hydrogen-methane blends
Decarbonization
Renewable fuels
Industrial furnace
Experimental trials

ABSTRACT

This study examines hydrogen as a low-emission alternative to natural gas in industrial furnace combustion, focusing on its well-known benefits of reducing carbon emissions and the technical challenges it presents. While decreasing carbon-based emissions with increased hydrogen content is well documented and serves as a primary motivation for its adoption, this work investigates the broader implications, particularly the increase in nitrogen oxide emissions, a significant contributor to air pollution, due to elevated combustion chamber temperatures. Experimental tests were conducted in a pilot-scale industrial furnace equipped with a burner operating at 42 kW, using pure methane, pure hydrogen, and various hydrogen-methane blends, over air-excess ratios ranging from 1.0 to 1.6. Temperature, heat transfer, pollutants, and radical-species emissions during combustion were measured using thermocouples, gas analyzers, spectroscopy, and optical imaging. Across the investigated air-excess range, carbon dioxide emissions decreased progressively by 10.5%, 18.8%, 45.3%, and 100% as the hydrogen content increased from 25% to 100% (relative to pure methane). In contrast, average nitrogen oxide emissions were maintained for a mixture of 25% of hydrogen, while they increased up to 28.5% for the blend with a 75% hydrogen content (relative to pure methane). Pure-hydrogen operation resulted in higher nitrogen oxide emissions, but these were partially mitigated by operating under lean conditions. Overall, hydrogen-enriched combustion supports decarbonization but can increase nitrogen oxide emissions, highlighting an important trade-off. Chemiluminescence analysis and visual diagnostics using RGB and Ultraviolet imaging further highlighted the qualitative differences between methane and hydrogen flames, with important implications for flame monitoring, real-time diagnosis of fuel composition, and safety in hydrogen-fired systems.

These findings improve understanding of hydrogen's role in industrial decarbonization and motivate the development of combustion strategies tailored to effectively control nitrogen oxide emissions.

1. Introduction

The industrial sector plays a vital role in modern economies; however, it is also one of the largest consumers of fossil fuels and a significant emitter of greenhouse gases (GHGs) [1], making it a key target for decarbonization. Traditional fossil fuels, including natural gas and coal, remain the predominant sources of energy, especially in applications that require high-temperature processes, such as steel production [2] and glass manufacturing [3]. Hydrogen has emerged as a promising alternative to fossil fuels [4] mainly due to its zero-carbon dioxide emissions, high energy content (120 MJ/kg) [5], and suitability for high-temperature industrial processes such as steel, glass, and cement production [6]. Although electrification is considered a promising decarbonization pathway for several industrial applications [7], technical limitations related to achievable temperatures and heat transfer characteristics can restrict its applicability in high-temperature furnace operation [8]. In this context, hydrogen combustion is widely recognized as one of the few viable alternatives for decarbonizing industrial furnaces operating at elevated temperatures [9]. When produced using low-carbon electricity, hydrogen can also contribute to reductions in lifecycle greenhouse gas emissions [5]; however, its effective implementation in industrial furnaces primarily depends on combustion performance, thermal characteristics and emission control [10].

In industry, hydrogen can be used as a pure fuel or blended with natural gas to facilitate a transition to decarbonization [11]. Hydrogen-

☆ This article is part of a special issue entitled: 'SDEWES 2025 - ECM' published in Energy Conversion and Management.

* Corresponding author.
E-mail address: jarroyo@fcirce.es (J. Arroyo).

https://doi.org/10.1016/j.enconman.2026.121350

Available online 14 March 2026

Nomenclature

CCD	Charge-coupled device
CH*	Methylidyne radical
C2*	Diatomic carbon (Swan bands)
GHGs	Greenhouse gases
H_2-DRI	Hydrogen-based Direct Reduction of Iron
HE	Heat exchanger
OH*	Hydroxyl radical
RGB	Red, Green, Blue
UV	Ultraviolet
VIS	Visible
λ	Air excess ratio, defined as actual air/fuel ratio divided by stoichiometric air/fuel ratio

natural gas blending has been experimentally demonstrated as a feasible near-term strategy in existing combustion systems [6], enabling emission reductions while maintaining flame stability and acceptable operational performance [12]. In parallel, blending hydrogen into existing natural gas networks has been identified as a policy-relevant near-term strategy for using hydrogen [13,14]. The feasibility of replacing fossil fuels with hydrogen is currently being studied in multiple sectors: in the steel industry, Hydrogen-based Direct Reduction of Iron (H_2-DRI) is a viable alternative to coal-based processes [16]; in the cement and glass industries [4], high-temperature hydrogen combustion is being tested as a substitute for fossil fuels [5]; and the chemical industry, which already produces and consumes large amounts of hydrogen as a feedstock or by-product of its processes, is an early adopter of hydrogen combustion technologies [17].

Despite its potential as a clean energy carrier [14], hydrogen combustion presents several technical challenges that are particularly relevant to industrial furnaces [13]. Key issues include fuel non-interchangeability due to the higher flame speed of hydrogen [19], which affects flame stability [15] and the performance of existing end-use equipment designed for natural gas [18,20]. Moreover, hydrogen combustion generally results in higher flame temperature than natural gas alone [21], particularly for pure or high hydrogen fractions, with direct implications in nitrogen oxides (NO_x) formation [22]. Experimental [6] and numerical studies consistently report increased NO_x emissions associated with elevated combustion chamber temperatures in hydrogen-rich combustion systems [15]. These emissions may be reduced through well-established strategies, such as pre-combustion, combustion, and post-combustion techniques [23], which may be adapted for hydrogen and hydrogen-natural gas blends [18]. Additional approaches, including oxy-combustion and oxygen-enriched combustion, which reduce the nitrogen content in the oxidizer, as well as flue gas recirculation, which lowers the combustion chamber temperature, are also under investigation to further control NO_x formation [24]. In addition, the lower volumetric energy density of hydrogen and the difference in the Wobbe Index compared to natural gas require adjustments to the fuel supply and storage infrastructure [14], which, in some cases, may affect energy delivery and performance [19].

Although research on pure hydrogen combustion and compatible equipment is advancing, the technology required for a complete transition to hydrogen in industrial furnace applications remains under development. There is extensive literature on hydrogen-fueled internal combustion engines [25]. Recent efforts have shifted towards the role of hydrogen in power generation equipment, such as gas turbines [22], and pilot-scale demonstrations and hydrogen-ready industrial equipment are emerging [26]. However, large-scale industrial deployment is still limited by technical barriers, including burner design optimization, material compatibility, updated safety protocols, and infrastructure adaptation. As a result, further research and engineering validation are crucial to ensure the reliable, efficient, and safe operation of industrial systems that use hydrogen as a primary fuel [27,28].

With regard to fuel mixtures, numerous studies have addressed the addition of hydrogen to natural gas in combustion systems, including laboratory burners and industrial equipment, and many contributions rely on Computational Fluid Dynamics (CFD) techniques to analyze temperature and emissions in industrial burners and furnaces [29]. In the case of furnaces, recent semi-industrial experiments have reported NO_x formation along with furnace temperature distributions for natural gas/hydrogen mixtures up to 100% H_2 [26], and other semi-industrial studies (often in flameless/oxyfuel configurations) focus on changes in heat transfer and radiation when switching from natural gas to hydrogen [30]. However, experimental datasets on the operation of air-fired furnaces that provide both chamber temperatures and regulated emissions in a systematic sweep of excess air at constant thermal power remain limited.

The present study presents the results of experimental tests conducted in an industrial-scale furnace burning various fuels, including methane, hydrogen, and their mixtures. The facility is fully instrumented, enabling the combined analysis of combustion chamber temperature and gas-phase emissions under controlled operating conditions. Tests were performed at a constant power of 42 kW and under different air/fuel ratios. This study investigates the effects of fuel composition and air-excess ratio on pollutant emissions and combustion chamber temperature. The main contributions of this work are: (i) experimental characterization of hydrogen and hydrogen-methane combustion in a pilot-scale industrial furnace under conditions relevant to industrial energy conversion; (ii) combined analysis of temperature and gas-phase emission measurements to assess combustion performance; and (iii) systematic evaluation of pollutant emissions as a function of air-excess ratio for different fuel blends. Based on this scope, Section 2 describes the experimental methodology; Section 3 presents and discusses the results, and Section 4 summarizes the main conclusions.

2. Methods

The following sections describe the pilot-scale facility, measurement instrumentation, and operating conditions.

2.1. Experimental setup

The experimental tests are conducted in an industrial-scale pilot test furnace designed to accommodate various gaseous fuels. The experimental setup comprises three main streams: (i) a gaseous fuel stream (mixtures of methane and/or hydrogen) supplied from cylinder racks and regulated by a specific fuel control panel, with mass flow measurement prior to injection into the burner; (ii) a combustion air stream supplied by a specific fan, equipped with temperature/pressure probes and mass flow measurement, which feeds the burner to control the excess air ratio; and (iii) a flue gas stream generated in the combustion chamber, which flows through the furnace and then through a heat exchanger before being expelled through the flue gas chimney. In addition, an independent air stream is driven through the cold side of the heat exchanger (HE) air circuit, with controlled inlet and outlet temperatures, and expelled to a specific HE air stack. The composition of the combustion gases is monitored by sampling probes connected to online gas analysers, while the furnace temperature is measured by multiple thermocouples distributed throughout the chamber. A schematic representation of the facility is provided in Fig. 1.

The furnace is equipped with an NBP BP M 5 GV S/70 high-to-medium-speed flexible diffusion burner, capable of delivering power in the 5–58 kW range when operating on natural gas. The gaseous fuels are supplied via two independent premixed gas bottle racks, sourced from a certified gas provider. One rack is dedicated to pure methane, and the other to hydrogen and hydrogen-methane mixtures. The gas supply system is fully equipped with flow conditioning and safety components,

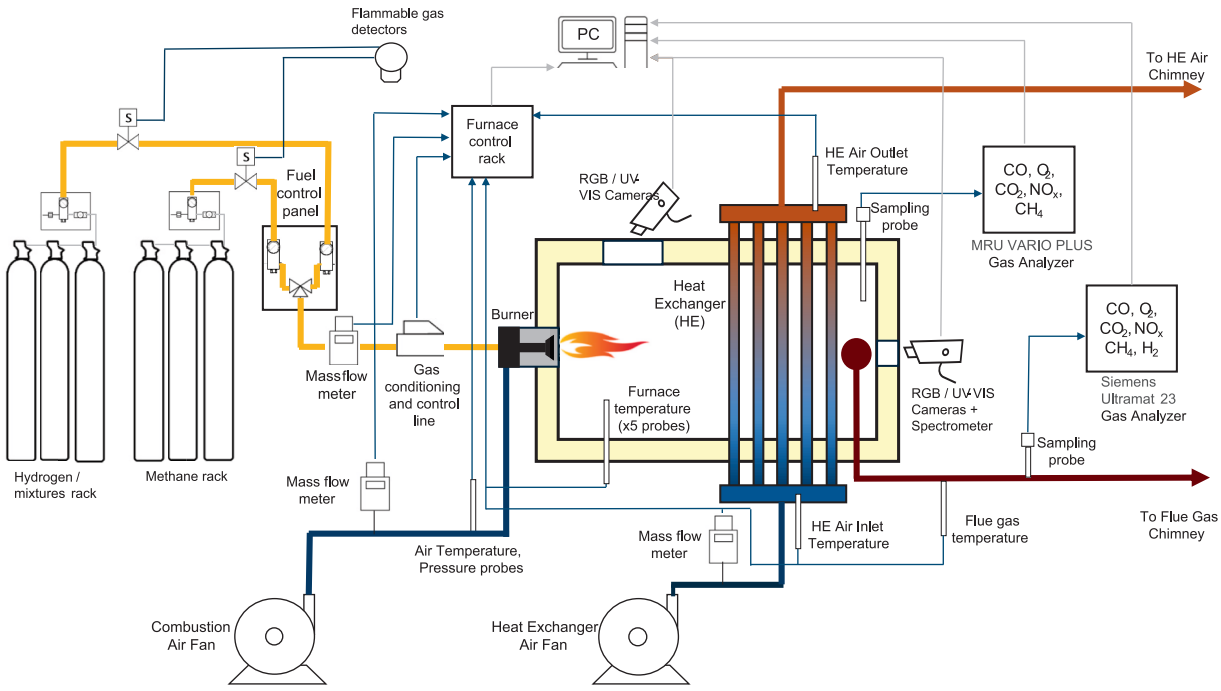

Fig. 1. Schematic of the experimental facility.

ensuring precise control over the gas flow. The fuel mass flow rate was measured using an Omega FMA-1611A mass flow meter, with an accuracy of ± 0.8% of reading plus ± 0.2% full scale. The combustion air is supplied by a forced-draft fan at an ambient temperature, and its flow rate was measured using a Sierra Instruments 620S fast-response insertion thermal mass flow meter, with an accuracy of ± 1% full scale and repeatability of ± 0.2% full scale. The internal furnace temperature is continuously monitored using five type S thermocouples. These thermocouples were positioned along the combustion chamber at 30 cm (T1), 60 cm (T2), 90 cm (T3), 120 cm (T4), and 150 cm (T5) from the burner mounting wall. Moreover, they were not positioned directly across from the burner head to avoid interference with the spectrum and image acquisition. The thermocouple radiation error was estimated by applying the radiation-loss approach for sheathed thermocouples, in which the measured junction temperature results from a steady-state balance between convective heat gain from the hot gases and radiative heat exchange with the surrounding enclosure/walls [31]. Following the methodology proposed for radiation-loss estimation in sheathed thermocouples, the temperature bias was computed from the coupled convection–radiation balance, yielding a correction (gas temperature minus indicated thermocouple temperature) in the range 15.1–31.8 °C under the present operating conditions.

The test furnace simulates an industrial process load using an air-cooled heat exchanger, which consists of a stainless-steel tube bundle arranged in a cross-flow configuration within the combustion chamber. During testing, the air flow is kept constant, with the heat dissipated ranging from 9 to 11 kW, depending on the conditions inside the combustion chamber. This setup allows for precise evaluation of heat transfer under varying operational conditions during each test. The system features inlet and outlet manifolds connected to the tubes via flexible silicone pipes, ensuring even airflow distribution. The airflow rate was recorded using a Sierra Instruments 620S mass flow meter (accuracy: ±1% full scale; repeatability: ±0.2% full scale), while the heat transferred to the load was determined using the flow rate measurement in conjunction with temperature readings from two Type K thermocouples placed at the inlet and outlet manifolds.

The composition of the combustion products is analyzed at two distinct locations within the system, utilizing two separate gas analyzers: inside the combustion chamber, at 210 cm from the burner wall, an MRU Vario Plus Industrial gas analyzer is employed to measure carbon monoxide (CO), oxygen (O_2), carbon dioxide (CO_2), NO_x, as nitrogen monoxide (NO) and nitrogen dioxide (NO_2) concentrations, and methane (CH_4), whose values are presented in this work. The measurement principles, ranges, and accuracies of these gas analyzers are summarized in Table 1. The measurement uncertainty of NO_x was determined point-by-point based on the specifications of the NO and NO_2 analyzers. For NO_x values below 100 ppm, the uncertainty remained approximately constant at 7.1 ppm, while for higher values, the combined uncertainty increased to 11.6 ppm (5.6% relative).

The second location is the flue gas chimney, 200 cm from the combustion chamber fumes outlet, where a Siemens Ultramat 23 gas analyzer provides additional measurements of CO, O_2, CO_2, NO_x, CH_4, and H_2. The data from the second analyzer are not used in this work and were primarily employed solely to ensure safety by mitigating risks associated with unburned gaseous fuel while also serving as a validation reference for the primary analyzer measurements.

All air and gas flow measurement instruments, as well as gas analysis equipment, have been calibrated by an accredited laboratory or possess the manufacturer's calibration certificate in the case of new equipment, ensuring that the uncertainty is within the specified ranges.

Table 1
Specifications of the gas analyzers.

Gas	Measurement Principle	Range	Accuracy
O_2	Electrochemical	0–21.0%v	± 0.2%v abs.
CH_4	Non-dispersive infrared (NDIR)	0–10000 ppm	± 60 ppm or 5% reading
CO	NDIR	0–10000 ppm	± 40 ppm or 5% reading
CO_2	NDIR	0–30%v	± 0.5% or 3% reading
NO	Electrochemical	0–1000 ppm (up to 5000 ppm)	± 5 ppm or 5% reading ≤ 1000 ppm 10% reading > 1000 ppm
NO_2	Electrochemical	0–200 ppm (up to 1000 ppm)	± 5 ppm or 5% reading ≤ 200 ppm 10% reading > 200 ppm

All measurement instruments and the furnace control rack are integrated into a central computer system, which continuously acquires and records data at a sampling frequency of 1 Hz.

The furnace is also equipped with two optical inspection quartz windows at the front and side of the combustion chamber. This allows direct visual access to the flame and transmission of ultraviolet (UV) radiation, facilitating optical monitoring. A portable spectrometer and four CCD cameras were installed at these locations to capture flame spectra and imaging data across both UV and visible (VIS) wavelength ranges, utilizing passband filters to isolate specific spectral regions. Table 2 summarizes the optical instruments used in the study, some of which are illustrated in Fig. 2. This figure also presents images of the test furnace and the visual setup installed in the two inspection windows. Regarding the optical equipment used, captures were made for all the operating points and fuels presented during the tests, of which a small sample is presented in this work. It is important to note that, throughout all the tests and under all conditions, both the exposure time and other camera lens parameters were kept constant in anticipation of future combustion monitoring algorithms based on computer vision.

The results are obtained from a series of trials with different hydrogen-methane blends, whose main characteristics are shown in Table 3. The measurement procedures during these trials are based on methodologies established in previous trials, which have led to the publication of several scientific studies [32,33].

The goal of using these mixtures is to evaluate furnace performance and emissions as the hydrogen percentage increases to 100%. Methane is used as a baseline fuel since it is the main component of natural gas, and hydrogen is used as a substitute fuel. The furnace operates at a constant thermal power of 42 kW for all tests, regardless of the fuel composition. The burner inlet gas pressure is regulated accordingly to maintain the required fuel flow rate, compensating for variations in the calorific value of different mixtures.

Methane was used during the preheating phase, which lasted approximately 6 h until the furnace reached a steady temperature. Once the furnace reached its nominal temperature, the fuel line was switched, and it began operating with the target test mixture. It was ensured that all residual gases in the combustion chamber were entirely replaced by those generated from the test fuel before taking measurements. Consequently, the measurements of the flue gas concentrations were stabilized.

Thus, the air excess ratio (λ), defined as the actual-to-stoichiometric air-to-fuel ratio, was systematically varied for each gas mixture, ranging from values close to stoichiometric conditions ($\lambda \approx 1$) to those close to combustion instability thresholds when combustion is fuel lean ($\lambda > 1$) by modifying the air flow rate, after which the furnace was stabilized for 10 min. Based on the operation and commissioning of the installation, it was verified that once steady-state operating temperature had been reached, following small changes in the airflow rate, the system attained its new steady state, verified by the stability in the mean oxygen concentration and in the temperatures, within these 10 min. Then, the variables were recorded over a 3-minute period, yielding 180 data points that constitute a representative sample for calculating the mean values reported in this study. During this period, spectra and images of all visual equipment were acquired.

Table 2
Equipment used in the inspection windows during the trials.

Equipment	Brand and model	Optical filter	Window	Exposure time
Spectrometer	Ocean Optics Flame-S Miniature	–	Frontal	1000 ms (integration time)
VIS RGB Camera	Imaging Source DFK 33GX174	–	Frontal	8.3 ms
(UV–VIS) Camera	Raptor Photonics Falcon Blue	310 nm ± 10 nm	Frontal	1000 ms
VIS RGB Camera	Jai GO-5000-PGE	–	Lateral	8.5 ms
(UV–VIS) Camera	EHD −704UV	310 nm ± 10 nm	Lateral	220 ms

3. Results and discussion

This section presents the experimental findings obtained from the combustion of the different fuel blends (Table 3). The results confirm a significant influence of both fuel composition and air-to-fuel ratio on the thermal behavior and flue gas emissions. Throughout the experimental campaign, the thermal power was kept constant, varying only the airflow rate supplied to the burner for each of the fuels studied to analyze the effect of excess or deficiency of oxidizer in the system. Fig. 3 shows the evolution of gaseous emissions of a) NO_x, b) CO_2, and c) CO as a function of the air-excess ratio.

Fig. 3 (a) shows NO_x emissions, calculated as the sum of the measured nitrogen oxides of the gas analyzers: $NO_x = NO + NO_2$. The analysis of the plots demonstrates that NO_x emissions (measured at 3% O_2, dry basis) increase with the hydrogen fraction, with the sensitivity to fuel composition being most pronounced near stoichiometric and slightly lean conditions. At λ values ranging from 1.10 to 1.15, NO_x levels remain within the range of 50–60 ppm for the $100CH_4$, $75CH_4$–$25H_2$, and $50CH_4$–$50H_2$ blends, but rise significantly to 80 ppm for the $25CH_4$–$75H_2$ blend (+60%) and reach 200 ppm for $100H_2$ (approximately 3.4 × the $100CH_4$ level).

In terms of the air-excess ratio, all fuel mixtures exhibit a maximum NO_x concentration at λvalues ranging from 1 to 1.10, which corresponds to conditions where the peak flame temperature is highest, thereby favoring thermal-NO_x formation via the extended Zeldovich mechanism [34]. The $100H_2$ case exhibits the highest peak NO_x values, reaching approximately 200 ppm, and remains distinctly elevated compared to the CH_4-containing blends in the near-stoichiometric region. This observation is consistent with the strong temperature dependence of thermal-NO_x formation and aligns with findings reported in [26]. As λ increases (indicating leaner operation), NO_x emissions decrease across all mixtures and converge to a range of approximately 50–70 ppm for $\lambda \geq 1.4$, indicating that lean combustion significantly diminishes the impact of the hydrogen fraction on NO_x emissions due to lower peak temperatures (thermal dilution) [26,35].

These results are consistent with previous studies, including those by Kikuchi et al. [24], who observed that using a burner designed for city gas led to a nearly 100% increase in NO_x emissions when operating with pure hydrogen compared to the original city-gas fuel. Additionally, studies by Schwarz et al. [26] have reported that replacing natural gas with hydrogen can increase dry NO_x emissions by approximately 38% under comparable firing conditions, with increases reaching 160–170% at specific operating points. These trends are in line with the observations made in the current study.

After normalization to 3% O_2, dry basis the measured CO_2 concentration (Fig. 3(b)), decreases monotonically with increasing H_2 fraction, while the influence of air excess ratio (λ) within the investigated range is comparatively small (typically < 0.5 vol% within a given blend). Averaged over the tested λ values, $100CH_4$ yields the highest CO_2 levels (9.1 vol%). Substituting CH_4 with H_2 produces stepwise reductions: $75CH_4$–$25H_2$ gives 7.6–7.9 vol% (8–12% reduction compared to $100CH_4$), $50CH_4$–$50H_2$ gives 6.7–7.3 vol% (15–23% reduction compared to $100CH_4$), and $25CH_4$–$75H_2$ gives 4.5–5.0 vol% (40–45% reduction compared to $100CH_4$). As expected, 100% H_2 results in CO_2 levels close to zero (≈ 0 vol%) across the whole λ range, corresponding to an ~ 100% reduction in direct CO_2 compared with CH_4. Overall, replacing 75% of CH_4 with H_2 cuts the corrected CO_2 concentration by roughly 3.5–4.0 percentage points, highlighting the strong potential of H_2 co-firing to reduce direct greenhouse-gas emissions in industrial thermal applications [36]. These results are consistent with those presented by other authors in experimental studies. For example, Bloj et al. observed a reduction in CO_2 emissions when using a $75CH_4$-$25H_2$ blend

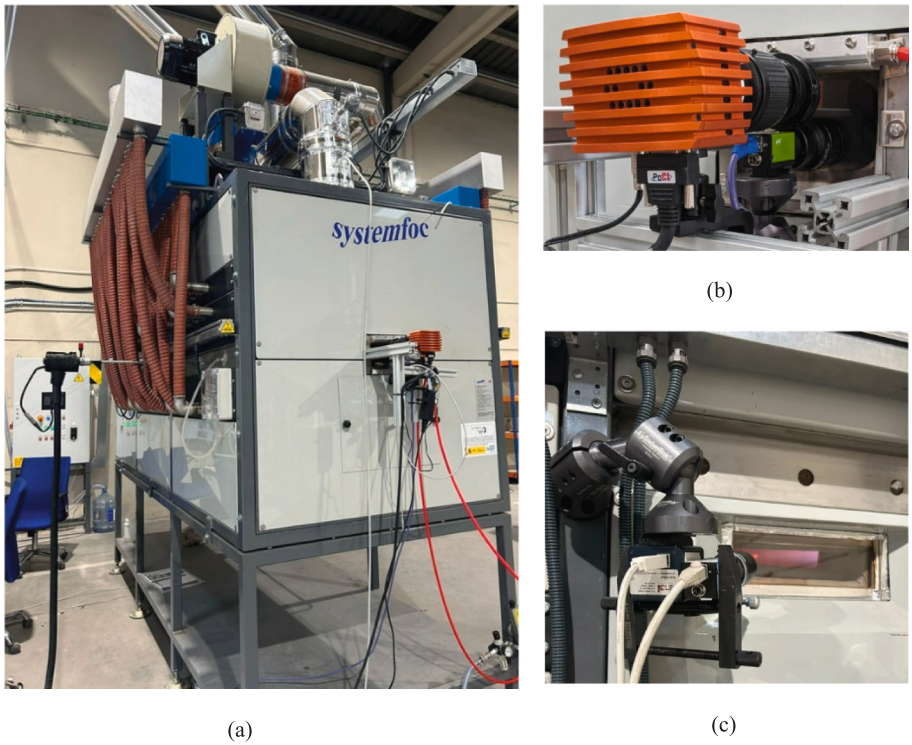

Fig. 2. (a) Furnace chamber, (b) camera setup from the front view with the Raptor Photonics Falcon Blue and the Jai GO-5000-PGE, (c) camera setup from the side view with the Imaging Source DFK 33GX174 and the EHD-704UV.

Table 3
Composition of the fuel blends used.

Mixture	CH_4 (% vol)	H_2 (% vol)	PCI (MJ/Nm^3)
$100CH_4$	100	0	35.85
$75CH_4$-$25H_2$	75	25	29.58
$50CH_4$-$50H_2$	50	50	23.31
$25CH_4$-$75H_2$	25	75	17.05
$100H_2$	0	100	10.78

compared to G222 gas (73% CH_4 − 23% H_2 by volume) [37].

Additionally, in [38], a reduction of 22.78% was reported when using a 50% CH_4 and 50% H_2 mixture, and a 46.96% reduction was observed with a 75% CH_4 and 25% H_2 blend, both of which align with the findings of the present study.

Fig. 3(c) shows that CO emissions (3% O_2, dry basis) are strongly localized around near-stoichiometric operation and become near-zero for λ approximately 1.05 for all fuel blends. This phenomenon typically occurs when the available oxygen is insufficient to achieve complete oxidation of the carbon in the fuel, or when localized regions of poor air–fuel mixing are present [39]. At λ approximately1.00, a distinct maximum is observed for CH_4-rich fuels: $100CH_4$ reaches 0.40 vol% CO, while blending H_2 markedly suppresses this peak to 0.08 vol% for $75CH_4$–$25H_2$ (80% lower than CH_4), 0.02 vol% for $50CH_4$–$50H_2$ (≈ 95% lower), and ≤ 0.01 vol% for $25CH_4$–$75H_2$ (≥ 97% lower). As expected, 100% H_2 yields negligible CO across the investigated λ range, consistent with the absence of carbon in the sharp reduction in CO with increasing λ reflects the transition from conditions where CO oxidation can be locally limited (e.g., marginal oxygen availability, finite residence time, and/or imperfect mixing near stoichiometric firing) to leaner conditions where excess oxygen and enhanced post-flame oxidation drive CO toward completion to CO_2. The systematic decrease in the near-stoichiometric CO peak as the H_2 fraction is primarily explained by the reduced carbon content in the fuel–gas mixture, while faster H_2-enriched kinetics and increased H/O radical availability further enhance CO to CO_2 conversion under the same global λ [40]. This dependence on excess air has also been reported by other authors, such as Jiang et al. in their industrial-scale experiments with methane–hydrogen mixtures [41], and by Huang et al. in their experiments comparing conventional combustion with MILD combustion in an experimental test furnace [42].

Based on emission trends, the best operating conditions would correspond to a value of λ between 1.1 and 1.2 in the case of methane and hydrogen-rich mixtures, since a controlled generation of NO_x is promoted, and CO emissions are eliminated while maintaining CO_2 generation (which remains very similar across the entire range of Lambda values). In the case of hydrogen, NOx emissions at these values are high, so it is recommended to increase the excess air to contain them, as the combustion kinetics of hydrogen allow for a broader range of excess air.

Fig. 4 illustrates the variation in the combustion chamber temperature at the thermocouple T1 location as a function of the excess air coefficient for the different fuel mixtures. The recorded temperature profiles reflect the combined influence of hydrogen content and air flow rate on combustion intensity. The peak T1 temperatures were observed under stoichiometric conditions (λ = 1) based on the experimental data, particularly in mixtures with higher hydrogen content. This effect is explained by the high enthalpy of combustion of hydrogen and its ability to intensify reactions in the primary combustion zone [43]. The maximum temperatures progressively decreased as the airflow increased (due to the dilution effect). Since the combustion gases contain more mass to heat due to the greater excess air and a significant amount of water vapor, the heat released is distributed over a larger heat load, resulting in lower temperatures as λ increases. In addition, hydrogen flames produce no soot or CO_2, so they radiate less than hydrocarbon flames, which may also contribute to lower temperatures measured by thermocouples. [44].

The temperature trends show a consistent coupling between the temperature measured at thermocouple T1 and NO_x formation. As λ increases, the temperature decreases and NO_x generally peak close to near-stoichiometric conditions before decreasing at higher λ. In

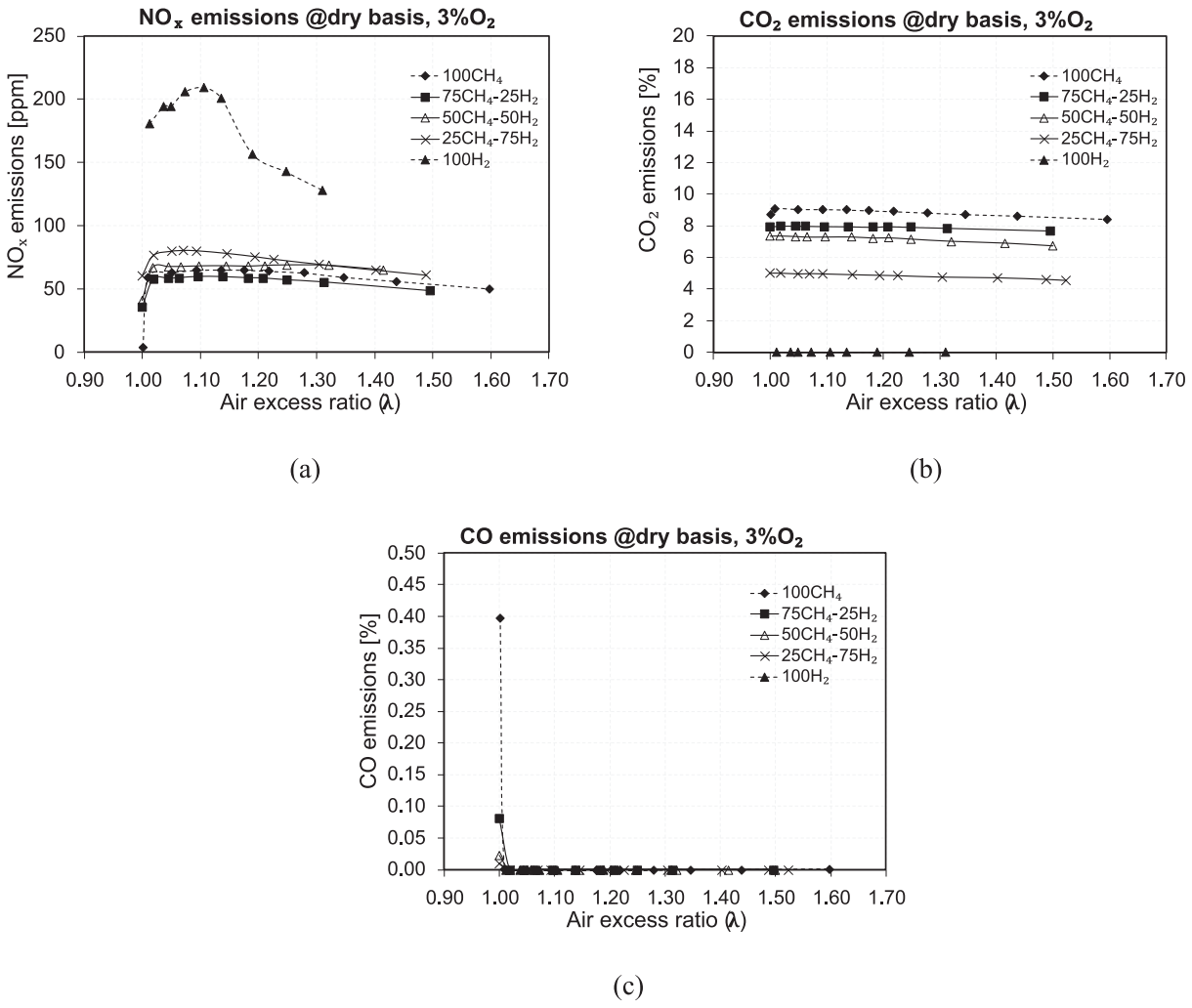

Fig. 3. Evolution of pollutant emissions versus air excess ratio (λ) standardized to 3% oxygen at dry conditions (a) NO_x, (b) CO_2, (c) CO.

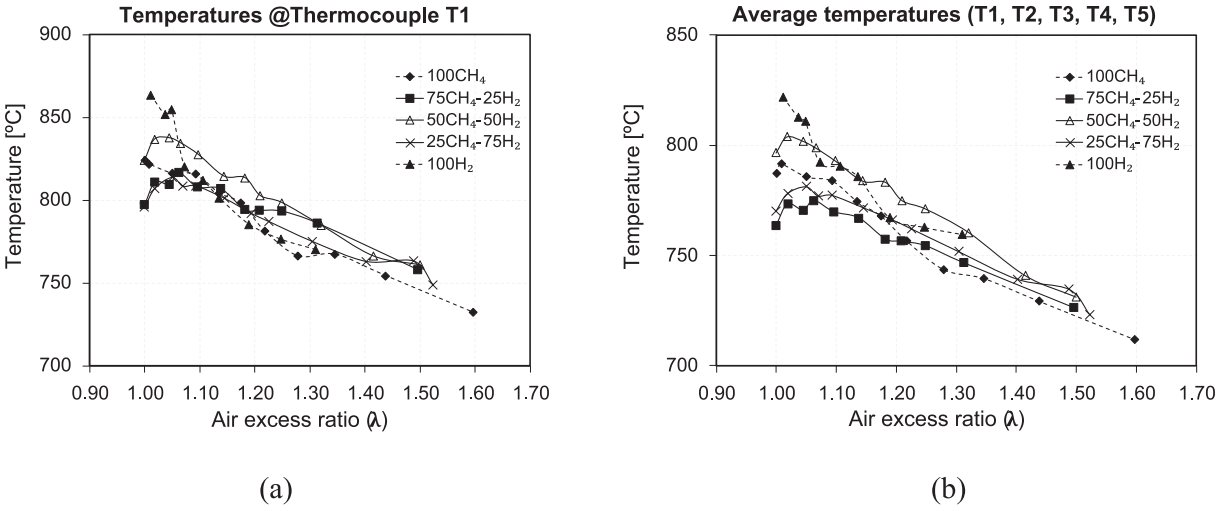

Fig. 4. Temperature inside the combustion chamber (a) in the first thermocouple, (b) average temperature of the five thermocouples.

addition, increasing the H_2 share shifts the operation towards higher temperatures near $\lambda = 1$ and correspondingly higher NO_x levels, with $100H_2$ case exhibiting the highest temperatures and the largest NO_x peak.

This temperature reduction, consistent with the decrease in NO_x emissions, highlights the importance of fine-tuning the aeration regime to balance efficiency and emission control.

Regarding chemiluminescence analysis, Fig. 5 presents the

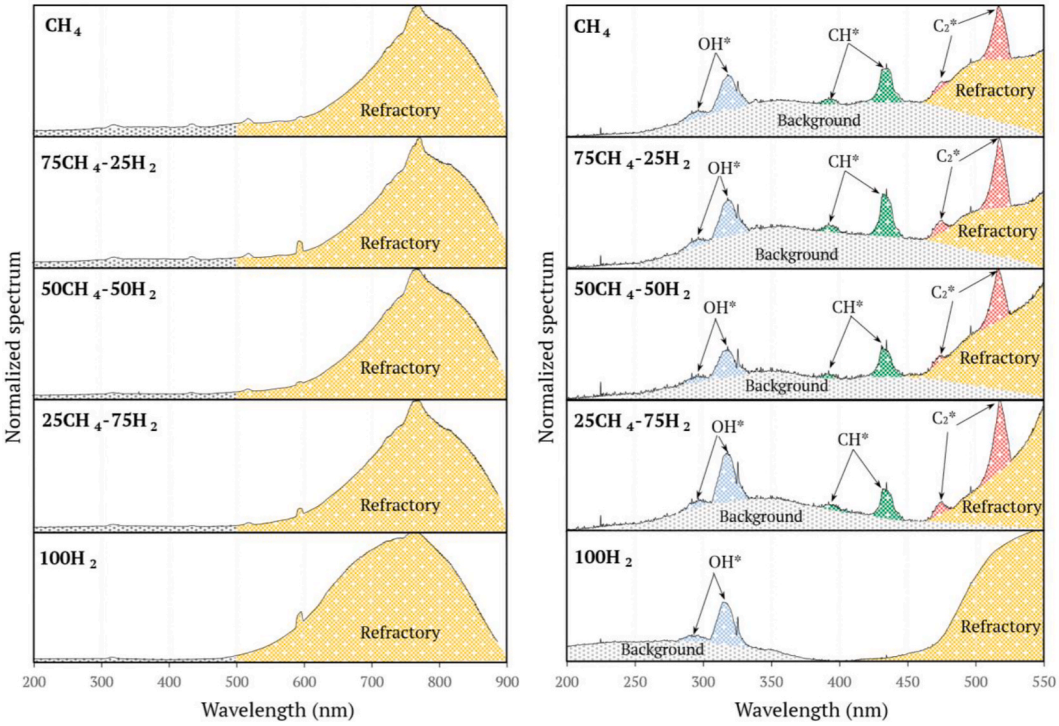

Fig. 5. Normalized average spectra for the different methane–hydrogen mixtures (a) from 200 nm to 900 nm and (b) from 200 nm to 550 nm.

normalized spectra obtained from the combustion of the different blends, displayed across the full spectrometer range (200 to 900 nm) in (a) and the 200–550 nm spectral window in (b). For each fuel type, the corresponding spectrum was generated by first averaging the spectral data over all measurement points, followed by min–max normalization of the resulting average spectrum.

In all cases, a pronounced broadband emission is observed in the 500–900 nm range, with intensity progressively increasing toward longer wavelengths. This portion of the spectrum is primarily associated with thermal radiation emitted by the burner and surrounding refractory materials, which operate at elevated temperatures and emit strongly in the orange, red, and near-infrared regions [45].

The observed increase in thermal radiation from the refractory zone with higher hydrogen content can be attributed to the shorter flame length characteristic of hydrogen combustion. Due to the high diffusivity and fast reaction kinetics of hydrogen, combustion reactions occur closer to the burner surface, resulting in a more compact and intense flame. This proximity imposes a greater thermal load on the burner and its surrounding refractory components, resulting in elevated surface temperatures. Since thermal radiation scales with the fourth power of temperature (as described by the Stefan–Boltzmann law), even modest increases in surface temperature may significantly enhance radiative emission in the visible and near-infrared spectra.

Conversely, methane-rich flames exhibit longer lengths, with combustion reactions occurring further downstream. This increased flame standoff distance reduces thermal interaction with the burner surface, resulting in lower temperatures in the refractory zone and, consequently, a weaker radiative contribution in the corresponding spectral region.

The analysis of Fig. 5 combined with that of Fig. 6, which shows the spectra obtained for the different mixtures at an approximate λ of 1.1, allows for the analysis of the distinct chemiluminescent peaks corresponding to combustion radicals OH*, CH*, and C_2*. In the OH* band (306–320 nm), indicative of high-temperature regions and flame front activity, hydrogen addition is expected to accelerate reactions, increasing local OH* concentrations, but overall OH* intensity decreases because methane plays a significant role in its formation [46] and, as the proportion of methane decreases, the OH* peak diminishes.

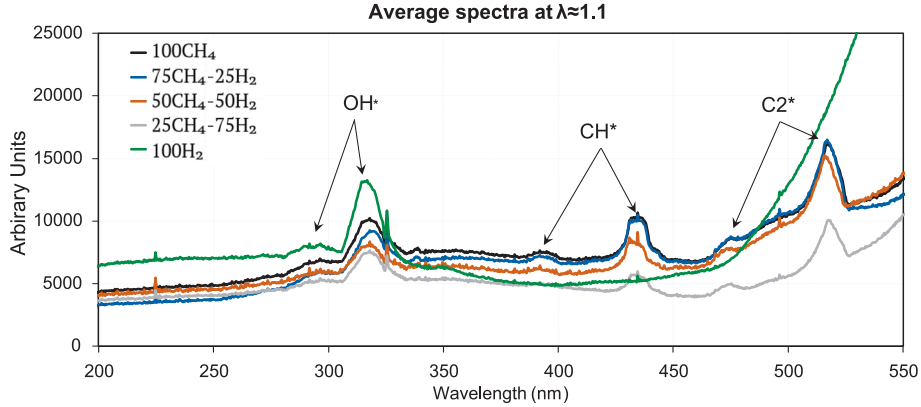

Fig. 6. Emission spectra of the different methane–hydrogen mixtures at an approximate air excess ratio of 1.1.

However, the OH * intensity peaks in $100H_2$ flames due to enhanced radical formation and faster combustion kinetics, which leads to a more turbulent flame in the area near the burner, as later verified in this study by analyzing the images captured with ultraviolet filters [47].

In contrast, the CH* band (428 nm), associated with hydrocarbon combustion, is prominent in methane-rich mixtures and its intensity decreases as the H_2 fraction in the mixture increases. Similarly, the C_2* Swan bands (~470–515 nm), markers of hydrocarbon breakdown and soot precursor activity, are strongest in CH_4-dominant blends and absent in H_2 flames [48,49]. Therefore, spectral trends confirm that hydrogen enrichment suppresses soot-forming pathways while promoting radical-driven combustion [50].

In addition to the quantitative results, RGB and UV images of the flames were obtained under the studied conditions, as shown in Fig. 7. The RGB images revealed significant visual differences between the mixtures. Flames with high hydrogen content appeared shorter, more stable, and reddish in hue, characteristics associated with higher temperature and reaction rate. On the other hand, flames of 100% CH_4 or low λ conditions exhibited a more yellowish and elongated coloration, indicative of areas with incandescent particles or incomplete combustion. Additionally, UV imaging visualized the emission of reactive species (OH*) associated with the chemical activity of the flame. These images were useful for identifying areas of high reactivity and confirming the combustion intensity in mixtures with a higher hydrogen content.

Fig. 7 visually compares the flames of $100CH_4$, $100H_2$, and a representative mixture ($50CH_4$-$50H_2$) under two distinct excess air coefficients: stoichiometric ($\lambda = 1$) and fuel-lean ($\lambda > 1$). RGB images illustrate variations in flame luminosity and structure. Hydrogen-rich flames exhibited higher luminosity and more distinct ring structures, particularly under richer conditions [51]. Ultraviolet (UV) imaging revealed the spatial distribution of reactive OH*, showing more intense and spatially extended chemiluminescence in flames of hydrogen, particularly in fuel-rich conditions. These results open up the possibility of potential combustion monitoring with these types of mixtures at an industrial level, using computer vision to monitor variations in the flame and even predict pollutant emissions.

4. Conclusions

Experimental findings confirm the feasibility of complete hydrogen combustion within existing industrial furnace infrastructure originally designed for natural gas. However, to accommodate the higher flame speed of hydrogen compared to methane, burner modifications are

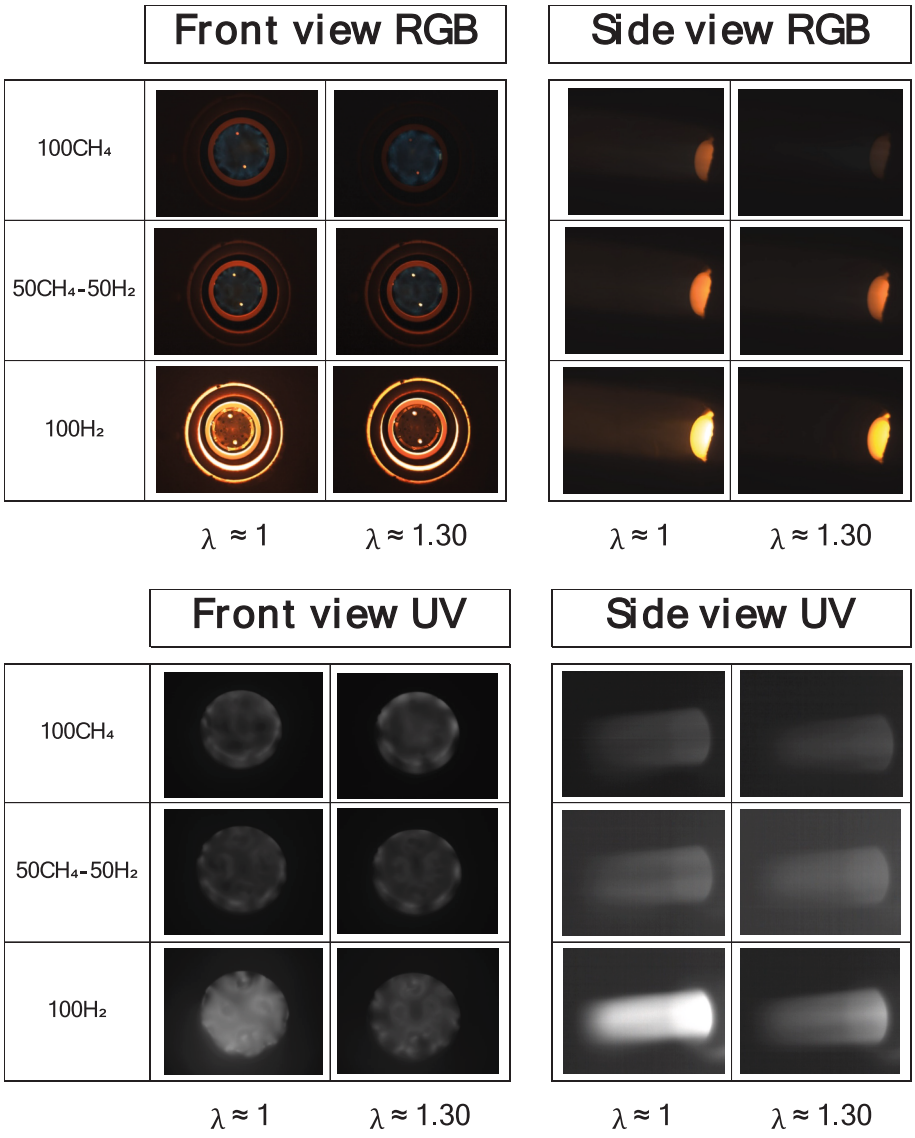

Fig. 7. RGB and UV combustion images, front and side views, for three different fuels: $100CH_4$, $100H_2$, and $50CH_4$-$50H_2$.

required to maintain flame stability and avoid liftoff, an issue commonly encountered due to hydrogeńs high diffusivity and reactivity.

As expected, a key finding is the strong inverse correlation between hydrogen content in the fuel mixture and carbon-based emissions. As hydrogen concentration in the fuel increases, both CO and CO_2 emissions decrease significantly, especially above 50%, with complete elimination under 100% hydrogen operation. This outcome, directly related to the absence of carbon in hydrogen, highlights its strong decarbonization potential when used as a full or partial substitute for methane in combustion systems.

In contrast, NO_x emissions rise significantly with increasing hydrogen content, reaching maximum values when the hydrogen content is 100%. This is attributed to the elevated combustion chamber temperatures characteristic of hydrogen combustion, which enhance thermal NO_x formation through the Zeldovich mechanism. Temperature measurements confirm this behavior: peak temperatures measured with the thermocouples located along the combustion chamber are observed under stoichiometric conditions ($\lambda = 1$), based on the data obtained during the tests. It should be noted that the measurements are relative, as the excess air coefficient was not experimentally tested for values less than 1. As the air flow increases beyond stoichiometric conditions, a progressive reduction in temperature is observed, which suggests that the heat transfer and combustion efficiency decrease with higher air supply. These thermal trends have direct implications for both emissions and heat transfer performance in industrial operations. These results highlight a significant challenge for the practical implementation of hydrogen in industrial settings and underscore the need for effective NOx control strategies, such as oxy-combustion, flue gas recirculation, or burner redesign.

Spectroscopic analysis through chemiluminescence revealed distinct differences in radical species based on fuel composition. Methane-containing mixtures exhibited characteristic emissions from C_2*, CH*, and OH*, while pure hydrogen combustion produced only the OH* signal. The OH* band (306–320 nm), indicative of high-temperature reaction zones, intensified with increasing hydrogen content, while CH* (428 nm) and C_2* (~470–515 nm) were only present in methane-rich flames. This confirms that hydrogen enrichment suppresses soot-forming hydrocarbon pathways while promoting radical-driven combustion. Additionally, a pronounced broadband emission in the 500–900 nm range was observed in all cases, primarily associated with thermal radiation from burner and refractory surfaces. As hydrogen content increased, the intensity of this radiation also increased. These findings not only verify the carbon-free nature of hydrogen flames but also validate chemiluminescence species as useful real-time indicators of fuel composition.

Finally, visual diagnostics using RGB and UV imaging further highlighted the qualitative differences between methane and hydrogen flames. Methane-rich flames were easily visible in the RGB spectrum, due to soot and carbon-based radiative emissions, whereas hydrogen flames appeared nearly invisible in the same range but exhibited strong signals in the UV spectrum associated with OH* chemiluminescence. This contrast has important implications for flame monitoring and safety in hydrogen-fired systems.

Overall, the results offer valuable experimental insights into the challenges and opportunities of hydrogen use in industrial thermal applications, laying the groundwork for future work focused on emission mitigation techniques and real-time diagnostic tools to enable the reliable and clean integration of hydrogen into industrial thermal systems. In particular, further research will aim to optimize burner geometries and apply advanced NO_x-control strategies (e.g., FGR, steam dilution, staged combustion, Oxy-hydrogen combustion and heat recovery) under dynamic industrial operating conditions. It will also develop cost-effective real-time optical diagnostics for flame/fuel monitoring and perform techno-economic and lifecycle assessments to evaluate hydrogen retrofitting feasibility across industrial sectors.

CRediT authorship contribution statement

Jorge Arroyo: Writing – review & editing, Writing – original draft, Visualization, Validation, Supervision, Resources, Methodology, Investigation, Formal analysis, Data curation, Conceptualization. **Fabiola Tovar-Lasheras:** Writing – review & editing, Writing – original draft, Visualization, Validation, Supervision, Software, Methodology, Investigation, Formal analysis, Data curation, Conceptualization. **Antonia Gil:** Writing – review & editing, Writing – original draft, Methodology.

Declaration of competing interest

The authors declare that they have no known competing financial interests or personal relationships that could have appeared to influence the work reported in this paper.

Acknowledgements

The work presented in this poster is part of the project H24NewAge, funded by the Cervera Network Research and Innovation Programme of the Spanish Ministry of Science and Innovation, under the CER-20211002 Grant Agreement.

Data availability

Data will be made available on request.

References

[1] Ademollo A, Mati A, Pagliai M, Carcasci C. Exploring the role of hydrogen in decarbonizing energy-intensive industries: a techno-economic analysis of a solid oxide fuel cell cogeneration system. J Clean Prod 2024;469:143254. https://doi.org/10.1016/j.jclepro.2024.143254.

[2] Jeswani HK, Zapata-Boada S, Spallina V, Azapagic A. Towards net-zero in steel production: Process simulation and environmental impacts of carbon capture, storage and utilisation of blast furnace gas. CCST 2025;15:100387. https://doi.org/10.1016/j.ccst.2025.100387.

[3] Jost D, Kanzurova S, Nilges B, Reinert C, von der Assen N. Life cycle assessment of measures towards a low-carbon flat glass production. J Clean Prod 2025;501:145294. https://doi.org/10.1016/j.jclepro.2025.145294.

[4] Hossain Bhuiyan MM, Siddique Z. Hydrogen as an alternative fuel: a comprehensive review of challenges and opportunities in production, storage, and transportation. Int J Hydrogen Energy 2025;102:1026–44. https://doi.org/10.1016/j.ijhydene.2025.01.033.

[5] Abbasian Hamedani E, Alenabi SA, Talebi S. Hydrogen as an energy source: a review of production technologies and challenges of fuel cell vehicles. Energy Rep 2024;12:3778–94. https://doi.org/10.1016/j.egyr.2024.09.030.

[6] Ravotti MA, Radünz C, Schwarz S, Demuth M, Canu P, Hochenauer C. Experimental study of the influence of oxygen enrichment in hydrogen-enriched natural gas combustion at a semi-industrial scale. Fuel 2026;405:1364. https://doi.org/10.1016/j.fuel.2025.136473.

[7] N. Schmitz N, Sankowski L, Kaiser K, Schwotzer C, Echterhof T, Pfeifer H. Towards CO2-neutral process heat generation for continuous reheating furnaces in steel hot rolling mills – a case study. Energy 2021;224:120155. https://doi.org/10.1016/j.energy.2021.120155.

[8] Diesing P, Blechinger P, Breyer C. Electrification versus hydrogen: a data-driven comparison framework for energy-intensive industries. Energy Convers Manag 2025;342:120145. https://doi.org/10.1016/j.enconman.2025.120145.

[9] Capurso T, Stefanizzi M, Torresi M, Camporeale SM. Perspective of the role of hydrogen in the 21st century energy transition. Elsevier 2022;251:114898. https://doi.org/10.1016/j.enconman.2021.114898.

[10] Wang Z, Lao G. Hydrogen production from renewable sources: bridging the gap to sustainable energy and economic viability. Int J Hydrogen Energy 2025;117:121–34. https://doi.org/10.1016/j.ijhydene.2025.03.176.

[11] Zhao C, Li X, Wang X, Li M, Xiao H. An experimental study of the characteristics of blended hydrogen-methane non-premixed jet flames. Process Saf Environ Prot 2023;174:838–47. https://doi.org/10.1016/j.psep.2023.04.041.

[12] Ersöz ME, Yolcan OO, Arat H, Erçetin Ü, Aydin O. Experimental investigation of hydrogen-enriched natural gas combustion in a domestic natural gas compatible boiler. Int J Hydrogen Energy 2026;199:152889. https://doi.org/10.1016/j.ijhydene.2025.152889.

[13] Levinsky H. Why can't we just burn hydrogen? challenges when changing fuels in an existing infrastructure. Elsevier 2021;84:100907. https://doi.org/10.1016/j.pecs.2021.100907.

[14] Erdener BC, Sergi B, Guerra OJ, Chueca AL, Pambour K, Brancucci C, et al. A review of technical and regulatory limits for hydrogen blending in natural gas

pipelines. Int J Hydrogen Energy 2023;48:5595–617. https://doi.org/10.1016/j.ijhydene.2022.10.254.
[15] Kim YB, Sohn CB, Jeong YS. Development of a low-NOx hydrogen combustion burner with an oblong flame port and orthogonal fuel-air injection. Appl Therm Eng 2025;279:127714. https://doi.org/10.1016/j.applthermaleng.2025.127714.
[16] Wang L, Wang G, Li S. Energy and exergy analyses of hydrogen direct reduction iron by the fluidized bed. Int J Hydrogen Energy 2024;80:779–87. https://doi.org/10.1016/j.ijhydene.2024.07.130.
[17] Zhen Z, Li B, Ou X, Zhou S. How hydrogen can decarbonize the chemical industry in China: a review based on the EIC–TER industrial assessment framework. Int J Hydrogen Energy 2024;60:1345–58. https://doi.org/10.1016/j.ijhydene.2024.02.001.
[18] Lewis AC. Optimising air quality co-benefits in a hydrogen economy: a case for hydrogen-specific standards for NOx emissions. Environ Sci: Atmos 2021;1:201–7. https://doi.org/10.1039/d1ea00037c.
[19] Franco A, Rocca M. Industrial decarbonization through blended combustion of natural gas and hydrogen. Hydrogen 2024;5:519–39. https://doi.org/10.3390/hydrogen5030029.
[20] González-Espinosa A, Gil A, Royo-Pascual L, Nueno A, Herce C. Effects of hydrogen and primary air in a commercial partially-premixed atmospheric gas burner by means of optical and supervised machine learning techniques. Int J Hydrogen Energy 2020;45:31130–50. https://doi.org/10.1016/j.ijhydene.2020.08.045.
[21] Ghazal RM, Akroot A, Abdul WA. Flame evolution characteristics for hydrogen/LPG co-combustion in a counter-burner. Appl Sci 2025;15:2503. https://doi.org/10.3390/app15052503.
[22] Ghazal RM, Akroot A, Abdul Wahhab A, Alhamd AEJ, Hamzah AH, Bdaiwi M. The influence of gas fuel enrichment with hydrogen on the combustion characteristics of combustors: a review. MDPI 2024;16:9423. https://doi.org/10.3390/su16219423.
[23] Skalska K, Miller JS, Ledakowicz S. Trends in NOx abatement: a review. Sci Total Environ 2010;408:3976–89. https://doi.org/10.1016/j.scitotenv.2010.06.001.
[24] Kikuchi K, Hori T, Akamatsu F. Fundamental study on hydrogen low-NOx combustion using exhaust gas self-recirculation. Processes 2022;10:130. https://doi.org/10.3390/pr10010130.
[25] Abubakar S, Muhamad Said MF, Abas MA, Ismail NA, Khalid AH, Roslan MF, et al. Hydrogen-fuelled internal combustion engines - bibliometric analysis on research trends, hotspots, and challenges. Int J Hydrogen Energy 2024;61:623–38. https://doi.org/10.1016/j.ijhydene.2024.02.280.
[26] Schwarz S, Daurer G, Gaber C, Demuth M, Hochenauer C. Experimental investigation of hydrogen enriched natural gas combustion with a focus on nitrogen oxide formation on a semi-industrial scale. Int J Hydrogen Energy 2024;63:173–83. https://doi.org/10.1016/j.ijhydene.2024.03.190.
[27] Zhang L, Li S, Liu T, Zhou H, Ren Z. Flow characteristics analysis and combustion oscillation mitigation of a hydrogen industrial burner. Int J Hydrogen Energy 2025;97:444–56. https://doi.org/10.1016/j.ijhydene.2024.11.402.
[28] Sekar M, Alahmadi A, Nithya S. Numerical simulation of industrial gas burners fueled with hydrogen-methane mixtures for enhanced combustion efficiency and reduced greenhouse gas emissions. Fuel 2024;370:131807. https://doi.org/10.1016/j.fuel.2024.131807.
[29] Bayramoğlu K, Yılmaz S, Bayramoğlu T, Özarslan A, Kılıç B, Akbay A. CFD-based evaluation of hydrogen–methane blends on temperature uniformity and emission control in ceramic furnaces. Int J Hydrogen Energy 2025;203:153176. https://doi.org/10.1016/j.ijhydene.2025.153176.
[30] Mabic K, Adendorff M, Madhu NT, Iplik E, Ekman T, Aslanidou I, et al. Heat transfer and emission characteristics of hydrogen-enriched natural gas in flameless air/oxyfuel combustion in a semi-industrial furnace. Energy 2026;9:100083. https://doi.org/10.1016/j.meaene.2025.100083.
[31] Roberts IL, Coney JER, Gibbs BM. Estimation of radiation losses from sheathed thermocouples. Appl Therm Eng 2011;31:2262–70. https://doi.org/10.1016/j.applthermaleng.2011.03.020.
[32] Arroyo J, Pérez L, Cuervo-Piñera V. CFD modeling and validation of blast furnace gas/natural gas mixture combustion in an experimental industrial furnace. Processes 2023;11:332. https://doi.org/10.3390/pr11020332.
[33] Compais P, Arroyo J, Tovar F, Cuervo-Piñera V, Gil A. Promoting the valorization of blast furnace gas in the steel industry with the visual monitoring of combustion and artificial intelligence. Fuel 2024;362:130770. https://doi.org/10.1016/j.fuel.2023.130770.
[34] Rao A, Liu Y, Ma F. Study of NOx emission for hydrogen enriched compressed natural along with exhaust gas recirculation in spark ignition engine by Zeldovich' mechanism, support vector machine and regression correlation. Fuel 2022;318:123577. https://doi.org/10.1016/j.fuel.2022.123577.
[35] Lan Y, Wang Z, Xu J, Yi W. The impact of hydrogen on flame characteristics and pollutant emissions in natural gas industrial combustion systems. Energies 2024;17:4959. https://doi.org/10.3390/en17194959.
[36] Sakib AN, Mehjabin F, Schmidt JB, Haque M, Saha K, Bhuiyan MMH. Harnessing hydrogen: a comprehensive literature review on strategic launching initiatives in the global energy market. Int J Energy Res 2024;2024:1–21. https://doi.org/10.1155/2024/3265065.
[37] Bloj MD, Ripeanu RG, Diniță A, Oprea VO, Tănase M. Comprehensive review of hydrogen-natural gas blending: global project insights with a focus on implementation and impact in Romanian gas networks. Heliyon 2025;11:e43090. https://doi.org/10.1016/j.heliyon.2025.e43090.
[38] Hammerstrom B, Niezrecki C, Hellman K, Jin X, Ross MB, Mack JH, et al. The viability of implementing hydrogen in the commonwealth of massachusetts. Front Energy Res 2022;10:1005101. https://doi.org/10.3389/fenrg.2022.1005101.
[39] Cellek MS. Flameless combustion investigation of CH_4/H_2 in the laboratory-scaled furnace. Int J Hydrogen Energy 2020;45:35208–22. https://doi.org/10.1016/j.ijhydene.2020.05.233.
[40] Yilmaz I, Ilbas M. An experimental study on hydrogen-methane mixtured fuels. Int Commun Heat Mass Transf 2008;35:178–87. https://doi.org/10.1016/j.icheatmasstransfer.2007.06.004.
[41] Jiang H, Lu L, Gong X, Tang Y, Qiu H, Feng Q. Influence of excess air coefficient variations on MILD combustion characteristics of CH_4/H_2 blends and associated NO/CO formation in industrial-scale furnace. Int J Hydrogen Energy 2026;204:153304. https://doi.org/10.1016/j.ijhydene.2025.153304.
[42] Huang M, Li R, Xu J, Cheng S, Deng H, Zhang B, et al. Effect of thermal input, excess air coefficient and combustion mode on natural gas MILD combustion in industrial-scale furnace. Fuel 2021;302:121179. https://doi.org/10.1016/j.fuel.2021.121179.
[43] Habib MA, Abdulrahman GAQ, Alquaity ABS, Qasem NAA. Hydrogen combustion, production, and applications: a review. Alex Eng J 2024;100:182–207. https://doi.org/10.1016/j.aej.2024.05.030.
[44] Guo J, Lu W, Zhang T, Liu Z, Im HG. Numerical investigation of radiation enhancement in hydrogen flames with hydrocarbon blending. Combust Flame 2026;283:114586. https://doi.org/10.1016/j.combustflame.2025.114586.
[45] Kathrotia T. Reaction Kinetics Modeling of OH*, CH*, and C2* Chemiluminescence. 2011. Available: https://doi.org/10.11588/heidok.00012027.
[46] García-Armingol T, Ballester J. Flame chemiluminescence in premixed combustion of hydrogen-enriched fuels. Int J Hydrogen Energy 2014;39(21):11299-307. https://doi.org/ 10.1016/j.ijhydene.2014.05.109.
[47] Daurer G, Schwarz S, Demuth M, Gaber C, Hochenauer C. Experimental and numerical analysis of industrial-type low-swirl combustion of hydrogen enriched natural gas including OH* chemiluminescence imaging. Int J Hydrogen Energy 2024;80:890–996. https://doi.org/10.1016/j.ijhydene.2024.07.119.
[48] Compais P, Arroyo J, Gozález-Espinosa A, Castán-Lascorz MA, Gil A. Optical analysis of blast furnace gas combustion in a laboratory premixed burner. ACS Omega 2022;7:24498–510. https://doi.org/10.1021/acsomega.2c02103.
[49] Vogel M, Bachfischer M, Kaufmann J, Sattelmayer T. Experimental investigation of equivalence ratio fluctuations in a lean premixed kerosene combustor. Exp Fluids 2021;62:93. https://doi.org/10.1007/s00348-021-03197-5.
[50] Kathrotia T, Riedel U, Seipel A, Moshammer K, Brockhinke A. Experimental and numerical study of chemiluminescent species in low-pressure flames. Appl Phys B 2012;107:571–84. https://doi.org/10.1007/s00340-012-5002-0.
[51] White B, Goktepe B, Marsh R, Morris S, Price A. Does swirl number affect the radiative and convective heat transfer from diffusion hydrogen-methane blended flames? Therm Sci Eng Prog 2025;61:103568. https://doi.org/10.1016/j.tsep.2025.103568.